NANO LETTERS

Letter

pubs.acs.org/NanoLett

Electronic Structure and Luminescence of Quasi-Freestanding MoS_2 Nanopatches on Au(111)

Nils Krane, Christian Lotze,* Julia M. Läger, Gaël Reecht, and Katharina J. Franke

Fachbereich Physik, Freie Universität Berlin, Arnimallee 14, 14195 Berlin, Germany

Supporting Information

ABSTRACT: Monolayers of transition metal dichalcogenides are interesting materials for optoelectronic devices due to their direct electronic band gaps in the visible spectral range. Here, we grow single layers of MoS_2 on Au(111) and find that nanometer-sized patches exhibit an electronic structure similar to their freestanding analogue. We ascribe the electronic decoupling from the Au substrate to the incorporation of vacancy islands underneath the intact MoS_2 layer. Excitation of the patches by electrons from the tip of a scanning tunneling microscope leads to luminescence of the MoS_2 junction and reflects the one-electron band structure of the quasi-freestanding layer.

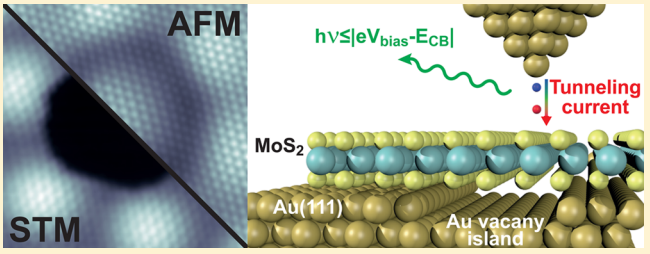

KEYWORDS: *Molybdenum disulfide, scanning tunneling microscopy, noncontact atomic force microscopy, photon emission*

Many two-dimensional (2D) materials and their heterostructures are currently discussed in a wealth of potential applications.[1,2] These are, for example, the transition metal dichalcogenides (TMDC), which exhibit semiconducting properties with an electronic band gap in the visible spectral range. The bulk materials of MoS_2, WS_2, $MoSe_2$, and WSe_2 are van der Waals-stacked crystals with an indirect band gap. When thinned down to a single layer, quantum confinement leads to a shift of the electronic bands and the emergence of a direct band gap at the *K*-point.[3,4] This leads to a drastic enhancement of photon absorption and photoluminescence efficiency. The optical properties are promising for the application of TMDCs in 2D photodetectors, sensors, or light-emitting devices.[5−7]

Devices made from 2D materials necessarily include interfaces to electrodes and substrates. However, interfaces strongly modify their electronic and optical properties. Hybridization of the chalcogenide states with the electronic states of the substrate leads to a change in the band structure.[8−10] In particular, it results in a reduction of the electronic and optical band gap. Whereas the electronic band gap is determined by the single-particle excitation by, e.g., a tunneling electron into or out of the TMDC, the optical gap is given by the excitation energy of an electron−hole pair. It is thus smaller than the electronic gap by the exciton binding energy. In TMDCs the exciton binding energy is extraordinarily large due to strong electron−hole correlation effects in 2D.[11,12] Excitons also play a role in many electroluminescence experiments across electrode−TMDC interfaces due to the simultaneous electron and hole injection at the junctions, which are subject to strong band bending.[13,14] The photon yield in these experiments is determined by both the exciton creation efficiency at the interface and the radiative relaxation efficiency, and is thus rather low. One may expect that electroluminescence does not necessarily underlie the requirement of exciton formation if the luminescence simply stems from the radiative relaxation of singly ionized states. For this, the challenge is to create a device where the charge injection barriers are not dominated by band bending. Metallic contacts with small Schottky barriers may be suited for this. However, such contacts often cause a low luminescence yield due to quenching of the excitation by the strong coupling of the charge carriers with the metallic states.

Here, we create monolayer islands of MoS_2 on Au(111), which include nanometer-sized patches with quasi-freestanding properties as evidenced by their electronic band gap. We ascribe this surprising behavior to the stabilization of Au vacancy islands below the MoS_2. We note that STM images in previous publications show apparent depressions reminiscent of the quasi-freestanding patches that we discuss here.[9,15] This suggests that the formation of vacancy islands is inherent to the growth process on Au(111). We excite these quasi-freestanding patches by electrons from the tip of a scanning tunneling microscope and detect the emitted photons. These arise from the radiative relaxation of the injected electrons into the quasi-freestanding MoS_2 layer.

The Au(111) substrate was cleaned by standard sputtering−annealing cycles under ultrahigh vacuum conditions. Molybdenum was deposited onto the clean Au(111) surface in a H_2S atmosphere of 10^{-5} mbar by electron-beam evaporation from a high-purity rod. Subsequently, the sample was annealed at 530 °C, a recipe adapted from Grøneborg et al.[15] The precooled samples were transferred into a CreaTec scanning

Received: May 24, 2016
Revised: July 26, 2016
Published: July 26, 2016

DOI: 10.1021/acs.nanolett.6b02101
Nano Lett. 2016, 16, 5163−5168

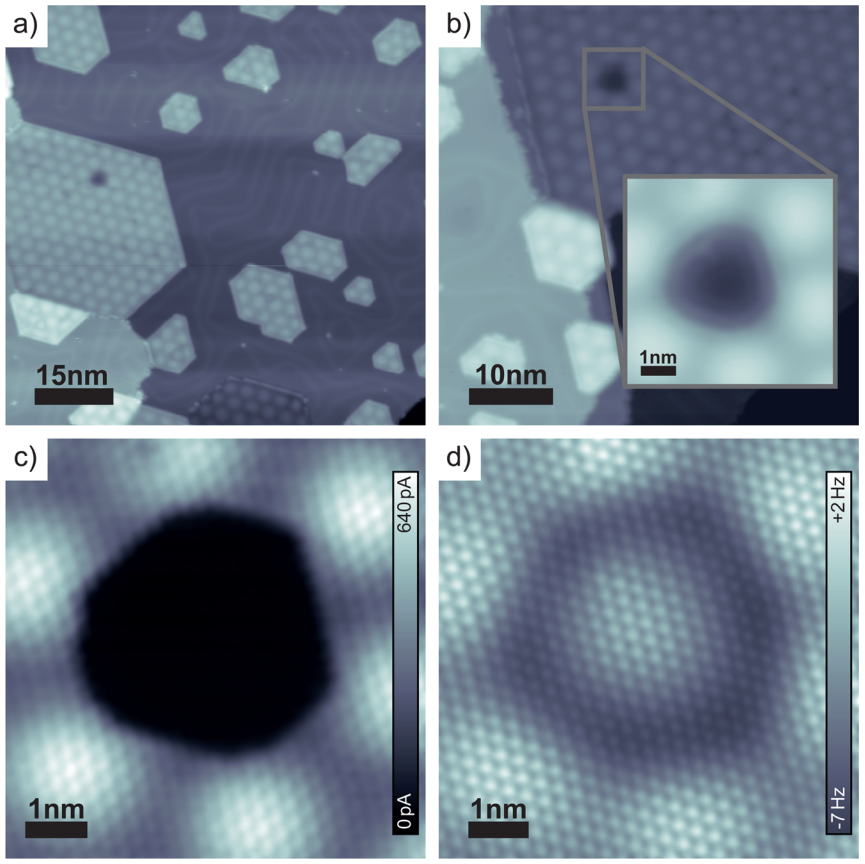

Figure 1. (a) STM topography overview image of MoS_2 on Au(111). The MoS_2 islands exhibit a moiré superstructure (V = 0.8 V, I = 100 pA). (b) Close-up STM image of a MoS_2 island with a pit. The inset shows a zoom into the MoS_2 pit (V = 0.8 V, I = 20 pA). (c) Constant-height tunneling current image on the inset region of the pit in (b). V = 5 mV, feedback loop was opened on the MoS_2 moiré at tunneling set point: V = 0.8 V, I = 200 pA and the tip was subsequently approached by 300 pm. (d) Constant-height AFM frequency-shift-image of the same region, taken simultaneously with (c). A Xe-functionalized tip was used to obtain resolution from repulsive short-range forces between tip and sample. The images were prepared using WSxM.[19]

tunneling microscope (STM) with a base temperature of 4.6 K. The microscope is equipped with a qPlus tuning fork sensor for combined measurements of tunneling and atomic force microsopy (STM/AFM).[16] Photons emitted from the tunneling junction were collected by an achromatic lens on the customized liquid helium radiation shield and guided through a mirror system out of the vacuum chamber.[17,18] A second achromatic lens is used to focus the light into a Princeton Instruments Acton SP-2150i spectrograph with a 150 lines/mm grating. Single photons are detected in the spectral range of 1.2 to 2.3 eV by a liquid-nitrogen-cooled Princeton Instruments Pylon 100BR eXelon spectroscopy camera. Scanning tunneling spectroscopy was performed using a lock-in amplifier (V_{mod} = 5.5 mV, f = 921 Hz). Light emission (LE) spectra were recorded in the constant-current mode at a set-point current of 10 nA and 100 s measurement time. To obtain maps of relative photon yield, we normalized all LE spectra to the Au surface plasmon spectrum, which was recorded at a sample bias of V = 3.5 V at the same acquisition settings.

In STM images (e.g., Figure 1a), single-layer MoS_2 islands appear with the typical hexagonal moiré structure of about 3.3 nm periodicity.[8,9] This structure is an expression of the lattice mismatch of the MoS_2 layer with the Au substrate (Figure 1b). In many of the islands we observe highly symmetric apparent depressions of several nanometer size when imaged at bias voltages below ∼0.9 V (see close-up view in Figure 1b). In the following we refer to these defects as "pits". In Figure 1c we show a tunneling current image at constant height reflecting the atomic structure of the upper sulfur layer of MoS_2. On top of the pit defect, however, the tunneling current vanishes at this tip−sample distance. Surprisingly, a simultaneously recorded AFM frequency-shift-image (Figure 1d), taken in the repulsive interaction regime with a Xe-functionalized tip, shows an unperturbed top sulfur layer, indicating an intact MoS_2 island. These observations lead to the conclusion that the hole-like topographic appearance in the STM images is of pure electronic origin.

We investigate the electronic properties of the moiré structure of MoS_2 and on top of the pit, at the points indicated by the crosses in Figure 2a), by recording dI/dV spectra (Figure 2b). The reference spectrum on the clean Au(111) surface (orange) is essentially featureless besides the onset of the surface state visible as a step at −490 mV. The width of the band gap of the MoS_2 layer is difficult to assign since we find a small tunneling contribution at all bias voltages. We hence use the logarithmically scaled spectrum for a more precise determination[11,20] of the band structure. The dI/dV spectrum shows an increase of conductance below about −1.6 eV and above about 0.9 and 1.4 eV. We compare these features with the calculated band structure of MoS_2/Au(111) in ref 8. The onset at negative bias fits well to the onset of the valence band at the Γ-point of the Brillouin zone. The onsets at positive bias

DOI: 10.1021/acs.nanolett.6b02101
Nano Lett. 2016, 16, 5163−5168

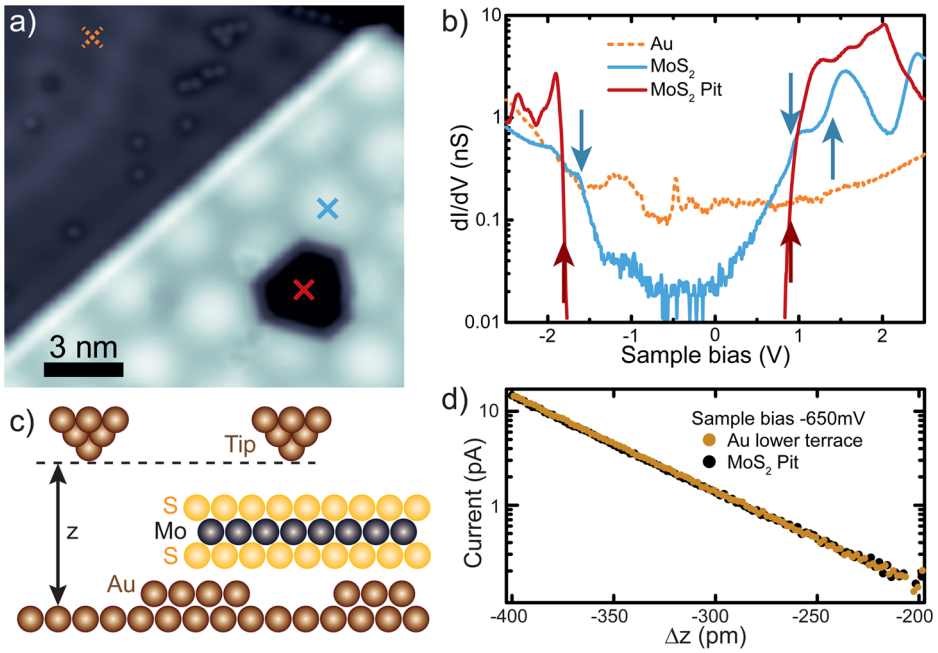

Figure 2. (a) STM image of MoS_2 on Au(111) with a pit defect and with crosses indicating tunneling spectroscopy locations (V = 0.1 V, I = 10 pA). (b) dI/dV spectra taken on Au(111) (orange), MoS_2 (blue), and the MoS_2 pit (red) as indicated by the colored crosses in (a). Arrows indicate the final states of photon emission corresponding to the lines in Figures 3 and 4. (c) Sketch of the structure model of the pit: MoS_2 overgrown on a Au vacancy island. (d) Current−distance ($I(z)$) curve on the pit and on a Au terrace, which is one step lower than the one supporting the MoS_2 layer. The current is equal at the same absolute tip height, suggesting the formation of a vacancy island below the pit.

agree with the minima of conduction bands at Γ. This band structure differs significantly from freestanding MoS_2 due to hybridization and screening with the metallic Au states.[8,12]

The dI/dV spectrum on the pit exhibits very different characteristics. The most obvious difference is a wider gap with sharp onsets of the conductance at around −1.8 and 0.9 V (red arrows in Figure 2b). The conductance within the gap is essentially zero, as one would expect it for a true electronic band gap. Spatially resolved dI/dV spectra across such a pit (see Supporting Information) show that the soft gap edges on MoS_2 abruptly sharpen and gradually shift away from the Fermi level. This evidences a sudden change of the hybridization of the probed bands with the Au states upon entering the pit area. Bruix et al.[8] have shown that the hybridization most strongly affects the sulfur states at the Γ-point, whereas it hardly influences the electronic bands at the K-point. Our technique is most sensitive to states at the Γ-point because the tunneling current is dominated by electrons with negligible $k_{\parallel}$ component. The observed shift of electronic bands at Γ thus suggests a loss of the hybridization with the Au substrate states and corroborates a picture of a decoupled MoS_2 layer, which is transparent to electrons at low energies. The local decoupling could either be due to intercalants, which break the hybridization, or to a missing Au layer. The most likely intercalant is excess S, which may also lead to a AuS alloy. In an attempt to increase the number or size of the pits, we prepared the Au(111) surface by a significant S coverage prior to MoS_2 growth. This did not have any effect on the MoS_2 islands. This result can be explained by the desorption of S at the elevated growth temperature of MoS_2.[21] Hence, we exclude S or AuS as a decoupling layer. The more likely scenario is the formation of vacancy islands underneath the MoS_2 layer. Vacancy formation may happen in two processes: On the one hand, the lifting of the herringbone reconstruction due to adsorbates may lead to the ejection of Au atoms from the surface layer and creation of vacancies.[22] Whereas the Au adatoms diffuse to the step edges, vacancies have a smaller mobility and thus only nucleate in vacancy islands. These are stabilized under the MoS_2 layer. On the other hand, deposition of Mo on Au(111) at elevated temperatures leads to the formation of a AuMo alloy. Oxidation by S pulls out the Mo from the alloy and leaves vacancies behind.[23] To test the idea of an overgrown Au vacancy island, we compare the conductance on the pit and on a Au(111) terrace, which is one atomic layer lower than the one that carries the MoS_2 island (sketched in Figure 2c). At the same tip height, we observe in both cases the same current at small bias voltage (Figure 2d). This suggest that the pits indeed represent an electronically transparent MoS_2 layer, with Au vacancy islands underneath.

To probe the luminescence properties of the MoS_2 layer and the pits we detect the photons emitted from the tunneling junction upon radiative relaxation of the electrons.[24] We record photon intensity spectra $I(h\nu)$ at different sample bias voltages at constant tunneling currents of 10 nA and compare them with the reference spectra on the bare Au surface $I_{ref}(h\nu)$. The spectral line shape on Au reflects different resonant modes of the localized surface plasmon,[25] with the number and location of the resonances being affected by the macroscopic tip geometry.[26]

At negative bias voltage the spectra on the moiré structure of MoS_2 (blue curve in Figure 3a) are essentially of the same shape as on Au, but of different intensity depending on the spectral range and bias voltage. The behavior on the pits is drastically different. We do not detect any photons with energies $h\nu > |eV_{bias} - E_{VB}|$ with E_{VB} being the onset of the valence band at about −1.8 eV. For the spectra at −3.5 V (red curve in Figure 3a), no photons are detected with higher energy than 1.7 eV.

DOI: 10.1021/acs.nanolett.6b02101
Nano Lett. 2016, 16, 5163−5168

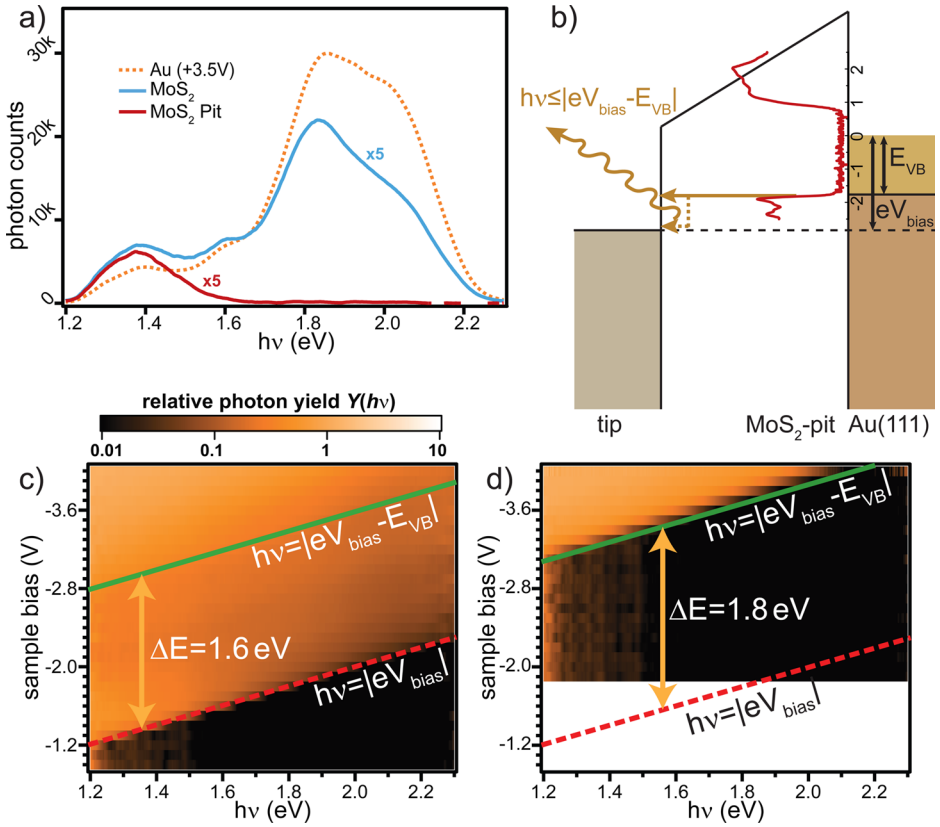

Figure 3. Photon emission at negative bias voltages: (a) Photon emission spectra recorded on the bare Au(111) surface (sample bias voltage V = +3.5 V), the MoS_2 layer, and a pit (both taken at sample bias voltage V = −3.5 V). (b) Model for STM induced photon emission on the pit at negative sample bias (see text). (c,d) Light emission maps recorded on the moiré structure of MoS_2 and a pit at negative sample bias (tunneling current I = 10 nA, 100 s acquisition time per sample bias). All spectra have been normalized to the gold tip surface plasmon, which was recorded at a sample bias of +3.5 V and same acquisition settings as denoted above. The red lines indicate the threshold $h\nu \leq eV_s$ of photon emission due to the applied bias voltage. The green lines indicate thresholds for the onset of photon emission processes due to the MoS_2 electronic band structure. On the pit we cannot record any spectra below −1.8 V because the density of states on the pit is so small that no electrons can tunnel from the occupied states of the sample. Only at larger negative bias voltages a finite tunneling current allows also for inelastic tunneling electrons, resulting in the excitation of localized surface plasmon-polaritons and, hence, the emission of photons.

To obtain a complete picture of the processes governing the photon emission, we plot, for both the moiré structure of MoS_2 and the pits, spectral maps of the relative photon yields $Y(h\nu) = I(h\nu)/S_{PL}(h\nu)$ where $S_{PL}(h\nu)$ is the surface plasmon enhancement function. $S_{PL}(h\nu)$ is derived from a reference spectrum recorded on the bare Au surface $I_{ref}(h\nu)$ for a bias V_{ref}, and corrected by the factor $(eV_{ref} - h\nu)^{-1}$, which accounts for the possible final states in the energy window set by the applied bias and the Fermi level.[18] Therefore, the relative photon yield $Y(h\nu)$ is independent of the surface plasmon modes. On the moiré structure of MoS_2, the onset of photon emission is found at $h\nu = |eV_{bias}|$ in Figure 3c). This onset marks the photon energy from the radiative relaxations of electrons originating from the Fermi level of the sample and relaxing in the junction to the Fermi level of the tip. A simple consideration of energy conservation does not allow for photons with larger energies. In the spectral maps presented here, we detect a small enhancement of the spectral yield above $h\nu = |eV_{bias}| - 1.6$ eV, which marks the onset of radiative transitions from electrons with their initial state at $E_{VB} = -1.6$ eV being the MoS_2 valence band. We observe no feature at constant photon energy, i.e., independent of the applied bias. Therefore, we can rule out, that radiative recombination of excitons or fluorescence processes occur in the junction.[27]

In contrast, the light emission maps recorded on the pits remain dark at large photon energies and only show intensity at photon energies $h\nu \leq |eV_{bias}| - 1.8$ eV (Figure 3d). Hence, radiative transitions of electrons originating from the Fermi level of the pit are absent. This is due to the lack of electronic states at the Fermi level and corroborates the picture of a freestanding MoS_2 nanopatch. Radiative transitions are only allowed for electrons tunneling out of the valence band[28,29] of the freestanding MoS_2 nanopatch, as indicated in the sketch in Figure 3b.

We now examine the luminescence properties at positive bias voltages. The spectral intensity in the LE spectra on the moiré structure of MoS_2 show slight differences compared with the LE spectra recorded on bare Au. For example, at a bias voltage of 3.5 V (see Figure 4a), the intensity on the moiré MoS_2 is higher below 1.9 eV and lower above. In contrast, on the pits, the photon emission is only enhanced for photon energies below 1.6 eV.

To again have a complete picture of the suppression and enhancement properties, we plot maps of the normalized spectral photon yield (Figure 4c,d). The spectral maps show several onsets of transitions, and again no feature at constant photon energy, excluding exciton and fluorescence processes. On the moiré structure, we identify three lines scaling with the bias voltage $h\nu = eV_{bias} - E_{final}$ with the final states being the

DOI: 10.1021/acs.nanolett.6b02101
Nano Lett. 2016, 16, 5163−5168

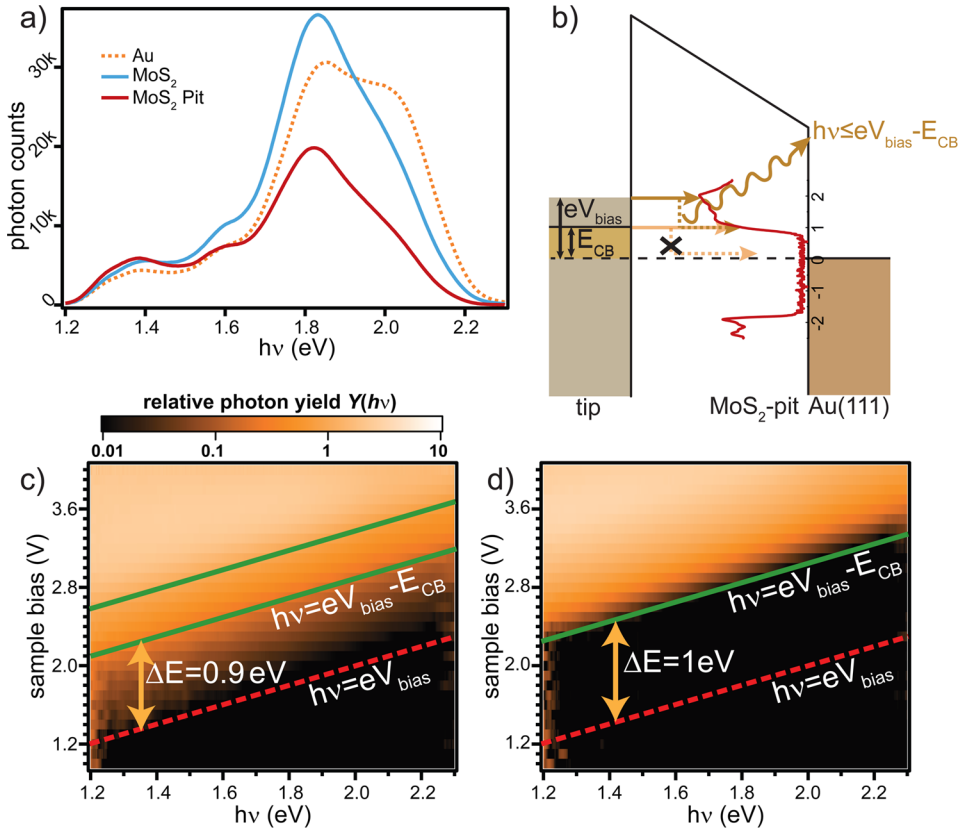

Figure 4. Photon emission at positive bias voltages: (a) Photon emission spectra recorded on the bare Au(111) surface, the MoS_2 layer, and a pit (all taken at a sample bias voltage V = +3.5 V). (b) Model of STM-induced light emission on the pit at positive sample bias. (c,d) Photon maps at positive sample bias on the moiré and the pit (tunneling current I = 10 nA, 100 s acquisition time per sample bias). All spectra have been normalized to the gold tip surface plasmon, which was recorded at a sample bias of +3.5 V and same acquisition settings as denoted above. The lines again indicate thresholds for photon emission processes. On the pit, light emission occurs with an offset of ∼1 eV: in order to emit photons, electrons must tunnel inelastically into a finite density of states, which exists only above the MoS_2−pit conduction band onset.

Fermi level, a state at 0.9 eV, and a second state at 1.4 eV. The latter two agree with the onsets of conduction bands around Γ, which we resolved also in the dI/dV spectra. Hence, photon emission is the consequence of inelastic tunneling electrons from occupied states of the tip to the MoS_2 conduction band at the Γ-point.

The LE spectra on the pits remain again dark in a larger photon energy range than on the moiré MoS_2. Only photons with energies $h\nu \leq eV_{bias} - 1.0$ eV are emitted (Figure 4d). The threshold of photon emission marks the onset of radiative transitions of inelastic tunneling electrons. At this threshold their initial state is the Fermi level of the STM tip and their final state is the conduction band of the pit at ∼1 eV (sketch in Figure 4b). The absence of photons with larger energies signifies the absence of states closer to the Fermi level, which would allow inelastic transitions. This proves again the lack of density of states in the band gap of the quasi-freestanding MoS_2 nanopatch.

With the combination of conductance and electroluminescence measurements, we have shown that during the growth of single-layer MoS_2 on Au(111) quasi-freestanding patches form, which are due to the stabilization of Au vacancy islands beneath the MoS_2 layer. Although our experiments are mainly sensitive to the electronic bands at the Γ-point, we do not suspect that there are strong modifications of the electronic structure at the K-point. The bands emerging at K exhibit a strong character of in-plane Mo 4d states and thus are largely unaffected by the interaction with the Au(111).[8] The role of the pit could thus be to prolong the exciton lifetime due to the decoupled character. Hence, it is interesting to further probe the excitons on the nanopatches by photoluminescence.

■ ASSOCIATED CONTENT

Supporting Information

The Supporting Information is available free of charge on the ACS Publications website at DOI: 10.1021/acs.nanolett.6b02101.

Spatially resolved differential conductance spectra and light emission spectra across MoS_2 "pit" (PDF)

■ AUTHOR INFORMATION

Corresponding Author

*E-mail: c.lotze@fu-berlin.de.

Notes

The authors declare no competing financial interest.

■ ACKNOWLEDGMENTS

We gratefully acknowledge funding by the German Research Foundation within the framework of the SFB 658, and the European Research Council for the ERC grant "NanoSpin".

■ REFERENCES

(1) Geim, A. K.; Grigorieva, I. V. *Nature* **2013**, *499*, 419−425.

DOI: 10.1021/acs.nanolett.6b02101
Nano Lett. 2016, 16, 5163−5168

(2) Wang, Q. H.; Kalantar-Zadeh, K.; Kis, A.; Coleman, J. A.; Strano, M. S. *Nat. Nanotechnol.* **2012**, *7*, 699−712.
(3) Mak, K. F.; Lee, C.; Hone, J.; Shan, J.; Heinz, T. F. *Phys. Rev. Lett.* **2010**, *105*, 136805.
(4) Splendiani, A.; Sun, L.; Zhang, Y.; Li, T.; Kim, J.; Chim, C.-Y.; Galli, G.; Wang, F. *Nano Lett.* **2010**, *10*, 1271−1275.
(5) Pospischil, A.; Furchi, M. M.; Mueller, T. *Nat. Nanotechnol.* **2014**, *9*, 257−261.
(6) Baugher, B. W. H.; Churchill, H. O. H.; Yang, Y.; Jarillo-Herrero, P. *Nat. Nanotechnol.* **2014**, *9*, 262−267.
(7) Ross, J. S.; Klement, P.; Jones, A. M.; Ghimire, N. J.; Yan, J.; Mandrus, D. G.; Taniguchi, T.; Watanabe, K.; Kitamura, K.; Yao, W.; Cobden, D. H.; Xu, X. *Nat. Nanotechnol.* **2014**, *9*, 268−272.
(8) Bruix, A.; Miwa, A. J.; Hauptmann, N.; Wegner, D.; Ulstrup, S.; Gronborg, S. S.; Sanders, C. E.; Dendzik, M.; Grubisic Cabo, A.; Bianchi, M.; Lauritsen, J. V.; Khajetoorians, A. A.; Hammer, B.; Hofmann, P. *Phys. Rev. B: Condens. Matter Mater. Phys.* **2016**, *93*, 165422.
(9) Sørensen, S. G.; Füchtbauer, H. G.; Tuxen, A. K.; Walton, A. S.; Lauritsen, J. V. *ACS Nano* **2014**, *8*, 6788−6796.
(10) Miwa, J. A.; Ulstrup, S.; Sørensen, S. G.; Dendzik, M.; Cabo, A. G.; Bianchi, M.; Lauritsen, J. V.; Hofmann, P. *Phys. Rev. Lett.* **2015**, *114*, 046802.
(11) Ugeda, M. M.; Bradley, A. J.; Shi, S.-F.; da Jornada, F. H.; Zhang, Y.; Qiu, D. Y.; Ruan, W.; Mo, S.-K.; Hussain, Z.; Shen, Z.-X.; Wang, F.; Louie, S. G.; Crommie, M. F. *Nat. Mater.* **2014**, *13*, 1091−1095.
(12) Qiu, D. Y.; da Jornada, F. H.; Louie, S. G. *Phys. Rev. Lett.* **2013**, *111*, 216805.
(13) Ye, Y.; Ye, Z.; Gharghi, M.; Zhu, H.; Zhao, M.; Wang, Y.; Yin, X.; Zhang, X. *Appl. Phys. Lett.* **2014**, *104*, 193508.
(14) Sundaram, R. S.; Engel, M.; Lombardo, A.; Krupke, R.; Ferrari, A. C.; Avouris, Ph.; Steiner, M. *Nano Lett.* **2013**, *13*, 1416.
(15) Grønborg, S. S.; Ulstrup, S.; Bianchi, M.; Dendzik, M.; Sanders, C. E.; Lauritsen, J. V.; Hofmann, P.; Miwa, J. A. *Langmuir* **2015**, *31*, 9700−9706.
(16) Giessibl, F. J. *Appl. Phys. Lett.* **2000**, *76*, 1470.
(17) Schulze, G. PhD Thesis, FU Berlin, 2009. http://www.diss.fu-berlin.de/diss/receive/FUDISS_thesis_000000016942.
(18) Stróżecka, A.; Li, J.; Schürmann, R.; Schulze, G.; Corso, M.; Schulz, F.; Lotze, C.; Sadewasser, S.; Franke, K. J.; Pascual, J. I. *Phys. Rev. B: Condens. Matter Mater. Phys.* **2014**, *90*, 195420.
(19) Horcas, I.; Fernandez, R.; Gomez-Rodrïguez, J. M.; Colchero, J.; Gomez-Herrero, J.; Baro, A. M. *Rev. Sci. Instrum.* **2007**, *78*, 013705.
(20) Bradley, A. J.; Ugeda, M. M.; da Jornada, F. H.; Qiu, D. Y.; Ruan, W.; Zhang, Y.; Wickenburg, S.; Riss, A.; Lu, J.; Mo, S.-K.; Hussain, Z.; Shen, Z.-X.; Louie, S. G.; Crommie, M. F. *Nano Lett.* **2015**, *15*, 2594.
(21) Biener, M. M.; Biener, J.; Friend, C. M. *Surf. Sci.* **2007**, *601*, 1659−1667.
(22) Poirier, G. F. *Langmuir* **1997**, *13*, 2019−2026.
(23) Biener, M. M.; Biener, J.; Schalek, R.; Friend, C. M. *Surf. Sci.* **2005**, *594*, 221−230.
(24) Lambe, J.; McCarthy, S. L. *Phys. Rev. Lett.* **1976**, *37*, 923.
(25) Johansson, P.; Monreal, R.; Apell, P. *Phys. Rev. B: Condens. Matter Mater. Phys.* **1990**, *42*, 9210.
(26) Meguro, K.; Sakamoto, K.; Arafune, R.; Satoh, M.; Ushioda, S. *Phys. Rev. B: Condens. Matter Mater. Phys.* **2002**, *65*, 165405.
(27) Qiu, X. H.; Nazin, G. V.; Ho, W. *Science* **2003**, *299*, 542.
(28) Geng, F.; Zhang, Y.; Yu, Y.; Kuang, Y.; Liao, Y.; Dong, Z. C.; Hou, J. *Opt. Express* **2012**, *20*, 26725.
(29) Schneider, N. L.; Matino, F.; Schull, G.; Gabutti, S.; Mayor, M.; Berndt, R. *Phys. Rev. B: Condens. Matter Mater. Phys.* **2011**, *84*, 153403.

DOI: 10.1021/acs.nanolett.6b02101
Nano Lett. 2016, 16, 5163−5168